Incorporation of MnO_2 Nanoparticles into MOF-5 for Efficient Oxygen Evolution Reaction

Muhammad Fiaz[a, b],Muhammad Kashif[a], Jafar Hussain Shah[a], Muhammad Naeem Ashiq[a], D. H. Gregory[b], Syeda Rabia Batool[c], Muhammad Athar[a*]

[a] Institute of Chemical Sciences, Bahauddin Zakariya University, Multan 60800, Pakistan

[b] WestCHEM School of Chemistry, University of Glasgow, Glasgow, G12 8QQ United Kingdom

[c] Institute for Chemical and Bioengineering, ETH Zurich, 8093 Zurich, Switzerland

[*]corresponding author: athar.qr@gmail.com

Graphical Abstract

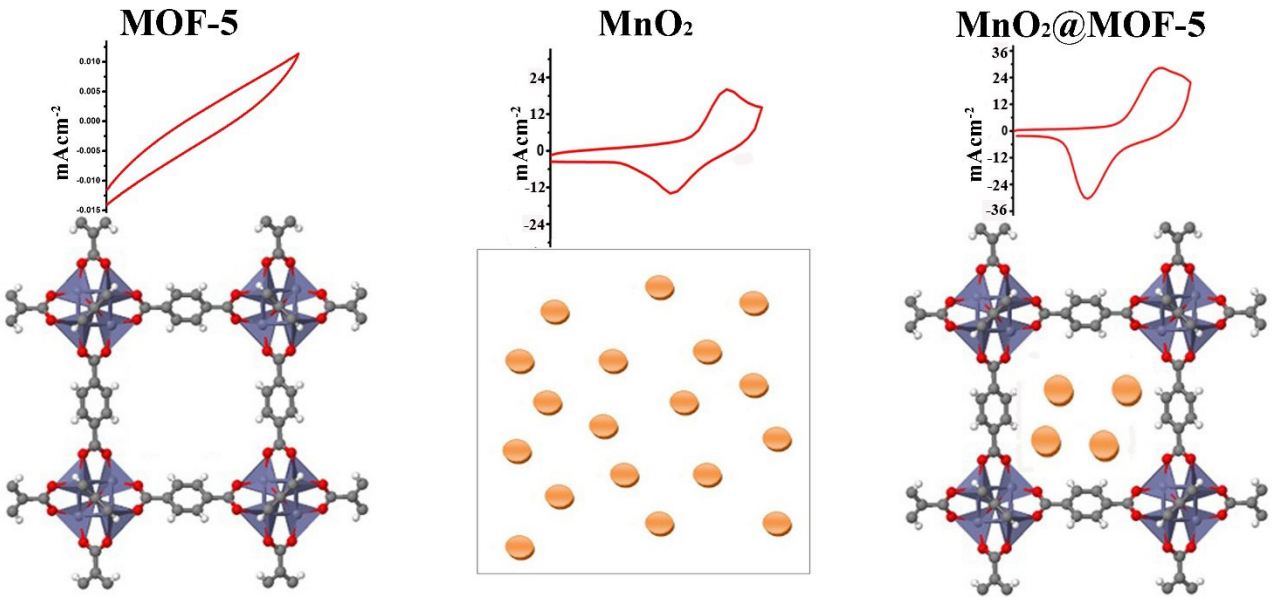

Abstract

A composite MnO_2@MOF-5 is prepared by in-situ incorporation of pre-synthesized MnO_2 nanoparticles into metal organic framework, MOF-5, during synthesis. The product is characterized by Powder X-Ray diffraction analysis, Raman spectroscopy, Fourier transform infrared spectroscopy, Ultraviolet-Visible spectroscopy, Scanning Electron Microscopy, Energy Dispersive X-ray spectroscopy and elemental mapping, which support the formation of proposed composite materials. The oxygen evolution reaction activity of MnO_2@MOF-5 composite is evaluated by cyclic voltammetry, linear sweep voltammetry and Chronoamperometric measurement under visible light. It is found that MnO_2@MOF-5/NF has better durability and ability to produce current density of 10 $mAcm^{-2}$ at only 324 mV overpotential with lower 71 $mVdec^{-1}$ Tafel slope as compared to some of previously reported Mn-based catalysts for OER. Stability of these electrodes is evaluated by Chronoamperometric studies for 6000 seconds in presence of visible light and they showed constant current density. Furthermore, stability studied by continuous CV sweeps in 1.0 M NaOH at a scan rate of 100 mVs^{-1} shows that these materials are stable upto 100 cycles, which confirms the stability and durability of the electrodes.

Key Words: MOF-5, MnO_2 nanoparticles, in-situ incorporation, Linear sweep voltammetry, Oxygen evolution reaction

Introduction

Increasing environmental pollution and rapid decrease of fossil fuels have diverted the attention of researchers towards the development of new alternate sources of energy [1]. Over the past few decades, many efforts have been made in this regard and it has been found that hydrogen can be used as a clean, secure, non-polluting and environment friendly source of energy [2]. Hydrogen can be produced from the hydrogen containing compounds like fossil fuels and biomass but they contaminate the environment [3]. Alternately, hydrogen can be effectively produced by photocatalytic water splitting which has no harmful effect upon environment [4]. The production of hydrogen by water splitting has attracted great attention after first reported by Fujishima and Honda in 1972 [5].

During water splitting, hydrogen and oxygen produced at surface of catalyst due to redox reaction [6]. Currently, Ru/Ir-based OER based catalysts have been emerged as best OER catalysts but due to their low earth abundant and high cost, they cannot be used at commercial levels [7-8]. So, development of highly active OER catalyst based on low cost earth abundant 3d-element has attracted a huge research attention. Therefore, up till now, more than hundred different materials have been reported as catalyst for water splitting [9]. However, high electron-hole pair recombination lowers the solar energy conversion and reduces the efficiency of catalysts [10]. Many efforts have been made to solve this problem but efficiency has not been increased up to satisfactory level [11].

In the recent years, metal organic frameworks (MOFs) have emerged as potential candidate for different applications such as storage [12], separation [13], catalysis [14] and biological imaging [15]. MOFs have unique properties such as high surface area and large number of cavities and channels [16]. In 2010, Garcia and co-workers reported Zr containing MOFs known as UiO-66 and UiO-66 (NH_2) as prominent catalysts for water splitting in the presence of visible light [17]. It has been observed that both UiO-66 and UiO-66 (NH_2) have greater catalytic activity towards water splitting when Pt nanoparticles are incorporated within the pores [18]. Since then many successful efforts have been made for preparation of composites of MOFs by incorporation of different materials such as metal/metal oxide nanoparticles [19], quantum dots [20], graphene [21], dense and porous silica nanospheres [22] and magnetic beads [23] to get specific properties. In MOFs, the organic ligands serve as antenna to harvest light and activate the metal. Photogenerated

electrons produced in MOFs are transferred to nanoparticles and increase the charge separation for efficient photocatalytic activity [24].

Manganese-based oxides (MnO_x) nanomaterials have been emerged as efficient OER catalysts due to their unique properties such as well-controlled morphology and electronic state [25-26]. Manganese oxide (MnO_2) nanoparticles, due to their stability, large surface area and small size [27] are used in redox reactions [28] and catalysis [29]. MOF-5 is an important metal organic framework that consists of $[Zn_4O]^{6+}$ clusters linked by octahedral arrangement of 1,4-Benzenedicarboxylate groups to form a cubic porous framework of MOF-5[30]. In the present work, nanoparticles of MnO_2 have incorporated into MOF-5 to form MnO_2@MOF-5 composite. Different experimental conditions are tested and composite materials showed superior OER performance to individual MnO_2 particles.

Experimental

Chemicals

The chemicals used for the synthesis of materials were zinc acetate dihydrate, $Zn(CH_3COO)_2.2H_2O$, 1,4-benzenedicarboxylic acid (H_2BDC), triethylamine (TEA), N,N-dimethylformamide (DMF), $KMnO_4$, $MnSO_4.H_2O$ and H_2O_2. All these chemicals were purchased from Merck. These were of analytical grade and used as such without any further purification.

Synthesis of MnO_2@MOF-5 Composite

Hydrothermal method was used for the preparation of nanoparticles of MnO_2 as reported in literature [31]. MnO_2@MOF-5 composite was prepared by incorporation of pre-synthesized nanoparticles of MnO_2 into MOF-5 during its synthesis. In a typical procedure, a suspension of 10 mg MnO_2 nanoparticles was prepared in 20 mL DMF. The suspension was added into 100 mL DMF solution containing 2.7g $Zn(CH_3COO)_2.2H_2O$. Then 50 mL DMF solution containing 0.8 g H_2BDC and 2 mL TEA was added dropwise to the mixture under constant magnetic stirring. The whole mixture was stirred at room temperature for 24 hours. The brownish precipitates were obtained and collected by centrifugation, washed with distilled water and DMF several times. The resulting product was dried at 50°C in vacuum oven for 3 hours and activated at 120°C for 6 hours. The dried precipitates were ground and stored for further characterization and photoelectrochemical studies. A sample of pure MOF-5 was also prepared by the same procedure without adding MnO_2 nanoparticles.

Oxygen evolution reaction studies

The oxygen evolution reaction studies of synthesized samples were studied in presence of visible light as well as in dark at room temperature by Cyclic voltammetry (CV), Linear sweep voltammetry (LSV) and Chronoamperometry using the electrochemical workstation (Autolab PG station 204) in 1.0 M NaOH aqueous electrolyte at various scan rates. The electrochemical measurements were conducted using a three-electrode setup containing Ag/AgCl as reference electrode and Pt-wire as counter electrode. All the applied potentials were converted into reversible hydrogen electrode (RHE) by using following equation

$$E_{RHE} = E_{Ag/AgCl\ /Sat.\ KCl} + 0.059\ pH + 0.197 \quad (1)$$

LSV was measured at 1 mVs^{-1} scan rate and it was used to evaluate Tafel plot according to following equation

$$\eta = a + b \log j \quad (2)$$

Where η is overpotential, j is current density and b is the Tafel slope. For OER overpotential was calculated by following equation

$$\eta = E_{RHE} - 1.23 \quad (3)$$

The working electrode was prepared on nickel-foam (NF). For the preparation of working electrode, a piece of NF (1cm × 1cm) was cleaned with ethanol and acetone by sonication for 30 minutes, respectively, washed with distilled water, and dried at room temperature. 10 mg of the prepared sample was added in distilled water to make the slurry, which was then uniformly pasted on NF and dried at 50°C for overnight. CV, LSV and Chronoamperometric measurements used the dried NF containing sample as working electrode for the study of water splitting activity. It was observed from SEM images that catalytic material remains deposited on the surface of Ni foam before and after photoelectrochemical reaction (Figure 1). It indicated the significant stability of these working electrodes for PEC studies.

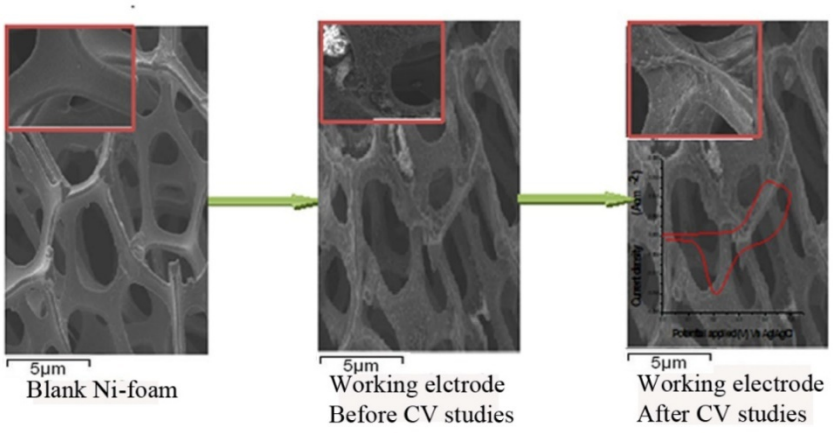

Figure 1: Schematic representation of coating on Ni-Foam and its use for photoelectrochemical study; inset are the magnify images of blank Ni-foam, Working electrode before CV studies and after CV studies

Characterization

Powder X-ray diffraction (XRD) patterns of pure MOF-5 and MnO_2@MOF-5 were recorded on a Shimadzu XRD diffractometer with Cu-Kα radiation (λ=0.15406nm) in the range of 2θ between 10° to 80° at scan rate of 5 degree min^{-1}. Raman spectrometry was carried by using Horiba Jobin-Yvon Lab RAM HR800 Raman Spectrometer in range from 100 to 2000 cm^{-1}. The 532 nm solid state laser was used to avoid florescence and decomposition of samples. Output power was reduced to 10% and acquisition time ranges from 5 to 10 minutes. Fourier transform infrared spectra were obtained by using Nicolet Nexus 870 in range from 4000-400 cm^{-1}.The morphology and composition of samples were studied by scanning electron microscopy (SEM) by using Philips XL30 Environmental SEM attached with Oxford Instrument Inca 500 Energy dispersive X-ray Spectrometer (EDX). The optical properties of the samples were studied by using Shimadzu UV-2600 UV-Visible spectrophotometer at room temperature in the range between 200 nm-900 nm.

Results and Discussion

Powder XRD patterns of MOF-5 and MnO_2@MOF-5 are shown in Figure 2, both the materials have grown in well crystalline form and intense peaks are observed. The P-XRD pattern of pure MOF-5 matches well with that reported in literature [32-33]. In the P-XRD pattern of MnO_2@MOF-5 the peaks that index to both MnO_2 and MOF-5 are observed and well defined diffraction peaks at 2θ about 19.18°, 20.47°, 30.52° correspond to MOF-5 and 13.55°, 18.61°, 28.45°, 38.65°, 41.11°, 50.13° to MnO_2. The diffraction peaks correspond to MnO_2 matches with

the standard XRD pattern ICSD 44-141. From the P-XRD patterns of MOF-5 and MnO_2@MOF-5, it is observed that the host MOF-5 maintains its characteristics reflection pattern and crystallinity.

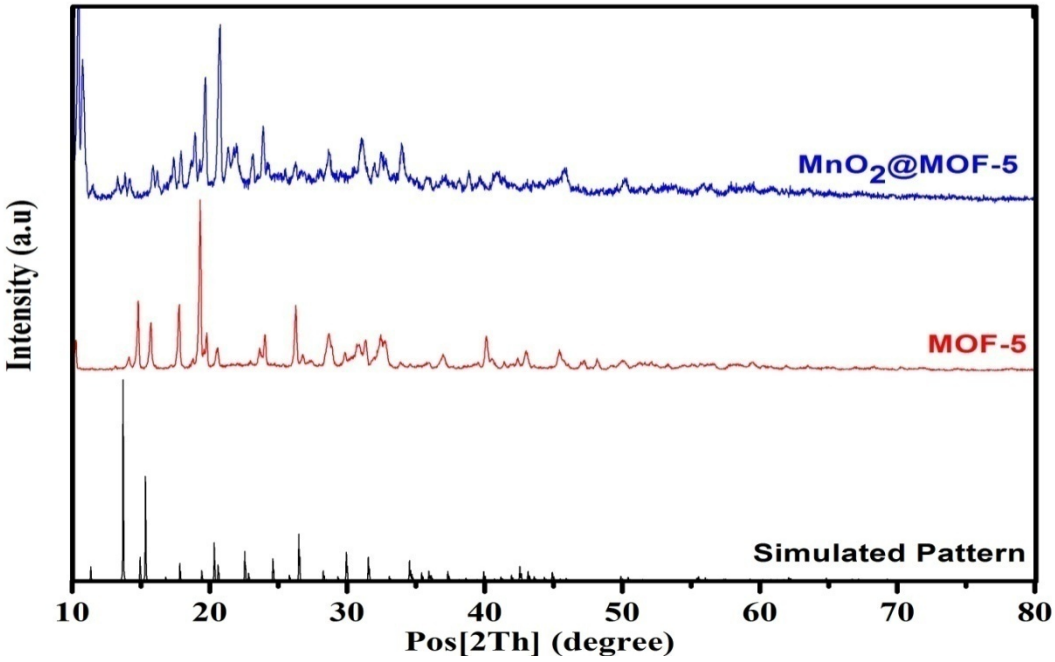

Figure 2: Powder XRD patterns of MOF-5and MnO_2@MOF-5 in comparison with simulated pattern of MOF-5

The Raman spectra of MOF-5 and MnO_2@MOF-5 are shown in figure S1 (supporting information). The Raman spectrum of MOF-5 consists of five strong Raman bands at 635 cm^{-1}, 865 cm^{-1}, 1139 cm^{-1}, 1448 cm^{-1} and 1615 cm^{-1} and these are in accordance with the results reported in literature [34]. These Raman bands are due to vibrational modes of benzene rings and vibration modes of carboxylate groups [35]. Similarly, the Raman spectrum of MnO_2@MOF-5 also consist of five Raman bands at 635 cm^{-1}, 865 cm^{-1}, 1141 cm^{-1}, 1434 cm^{-1} and 1615 cm^{-1}, which indicates that MOF-5 shows its dominance and maintain its crystalline structure. In Raman spectrum of MnO_2@MOF-5 slight Raman shifts can be observed at 1141 cm^{-1} and 1434 cm^{-1} which may be due to interaction of MnO_2 with $[Zn_4O]^{6+}$ clusters of MOF-5 and some displacement of organic ligand.

These five vibrational modes of MOF-5 and MnO_2@MOF-5 are comparable with DFT quantum calculations of MOF-5as reported previously [36]. The Raman spectra of MnO_2@MOF-5 does not contain characteristic peaks of MnO_2 because of dominance of host MOF, peaks of MnO_2 are masked.

FTIR spectra of both MOF-5 and MnO_2@MOF-5 are shown in figure S2. The FTIR spectra of MOF-5 shows two sharp vibrational peaks at 1575 cm^{-1} and 1370 cm^{-1} due to symmetric and

asymmetric stretching vibration of C-O whereas MnO_2@MOF-5 shows vibrational bands at 1586 cm^{-1} and 1377 cm^{-1} due to symmetric and asymmetric stretching vibration of C-O bonded to Zn, respectively. In the FTIR spectra of MOF-5, symmetric stretching vibration of Zn_4O appears at 642 cm^{-1} [37]. A strong peak appears at 530 cm^{-1} in FTIR spectrum of MnO_2@MOF-5 which may be due to overlapping of Mn-O vibration with secondary building unit of MOF-5, coordinated $[Zn_4O]^{6+}$ cluster.

The morphology and composition of MOF-5 and MnO_2@MOF-5 was studied by scanning electron microscopy and SEM based EDX, respectively. The SEM images are shown in figure 3, which shows that MOF-5 has grown in crystalline form having rectangular shape (Figure 3(a-b)). Figure 3(d-e) shows the SEM images of MnO_2@MOF-5 composite which indicates that MnO_2@MOF-5 also have morphologically smooth surface of the crystals. The EDX spectrum of MOF-5 and MnO_2@MOF-5 are shown in figure 3c and 3f, respectively. Figure 3c shows that the EDX spectrum of MOF-5 contains all the three elements (Zn, C and O) of MOF-5. Similarly, figure 3f shows that EDX spectrum of MnO_2@MOF-5 composite contain all the four elements (Zn, Mn, C and O) and indicated successful incorporation of MnO_2 into MOF-5.

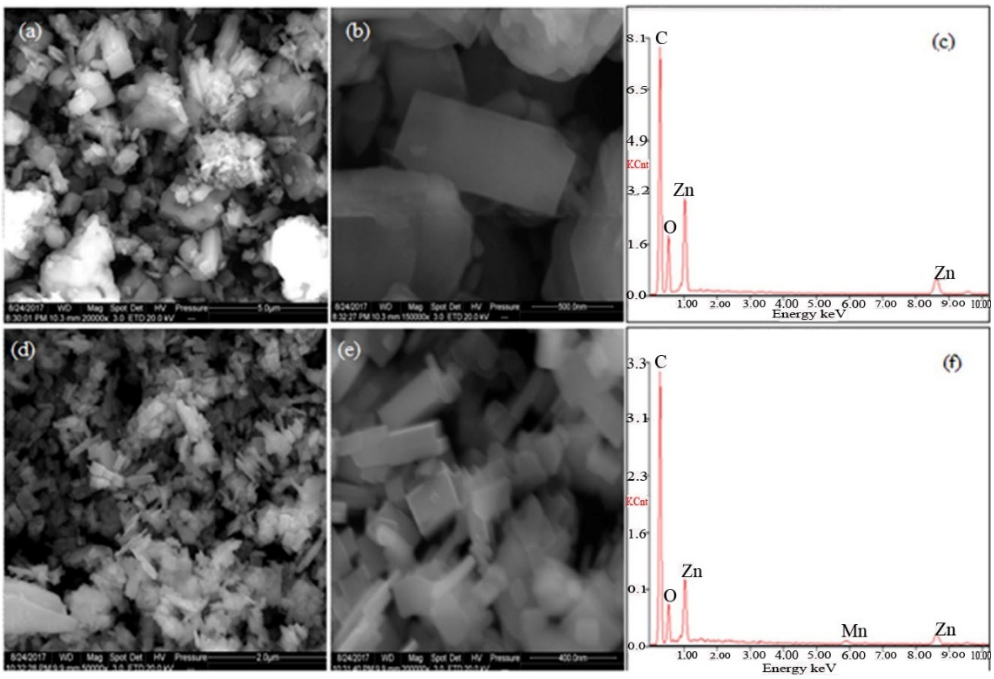

Figure 3: (a-b) SEM images, (c) EDX of MOF-5and (d-e) SEM images, (f) EDX of MnO_2@MOF-5

The elemental mapping analysis of MOF-5, as shown in figure 4(a-d), shows that there is uniform and homogeneous distribution of elements and it has grown in rectangular shape. The Figure 4a-4c

show elemental mapping of MOF-5 for Zn, C and O respectively and 4d is the mix mapping of metal organic framework, MOF-5, which indicated that all the basic elements are uniformly and homogenously distributed in the sample. Similarly, figure 4e-4g show elemental mapping of MnO_2@MOF-5 for Mn, Zn and O respectively and 4h is the mix mapping of MnO_2@MOF-5, which indicated that nanoparticles of MnO_2 has been successfully incorporated within MOF-5 as it can be observed that Mn is uniformly distributed in the composite.

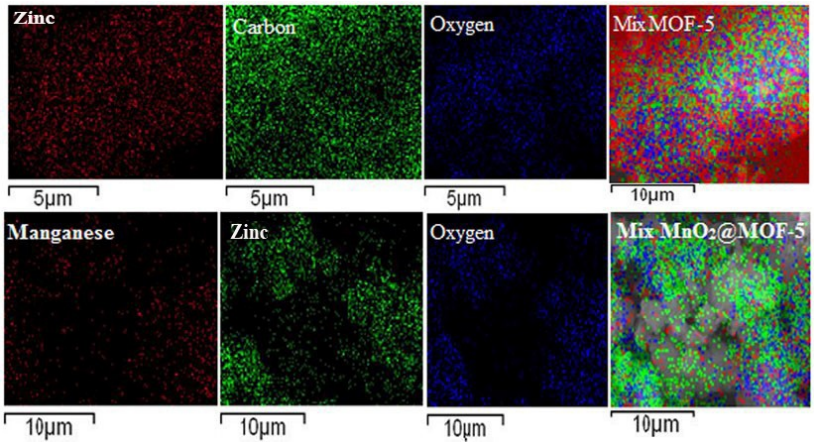

Figure 4: Elemental mappings of MOF-5and MnO_2@MOF-5

The optical properties of synthesized samples were studied by UV-Visible absorption spectrophotometry. As shown in figure S3, MOF-5 has maximum absorption in UV-region at 265 nm due to $\pi \rightarrow \pi^*$ electronic transition of 1,4-BDC linkers and with no significant absorption in visible light. After incorporation of MnO_2 into MOF-5, its λ_{max} shifts from 265 nm to 275 nm. Furthermore, a new absorption peak having λ_{max} around 400 nm has introduced with increase in absorption in the visible region. Such a modification increases the charge separation because photogenerated electron efficiently transfer from organic ligand 1,4-BDC to $[Zn_4O]^{6+}$ clusters of MOF-5 and then to MnO_2, similar to UIO-66(NH_2) and Ti-MOF-NH_2. The increase of charge separation has improved the photoelectrochemical activity. The band gap of a semiconductor can be calculated from Tauc plot by linear extrapolation of absorption edge by using following equation

$$\alpha h\nu \propto (h\nu - E_g)^{0.5} \qquad (4)$$

Where α=absorption coefficient, h= Planck's constant, ν= wavenumber

The band gap of MOF-5 is determined to be 3.70 eV, which is in accordance with literature reported previously [38]. While the band gap of MnO_2@MOF-5 is 2.47 eV, which indicated that incorporation of MnO_2 nanoparticles brings the band gap of MOF-5 into visible region. Hence, it increases the absorption of visible light and improves the photoelectrochemical activity of

MnO_2@MOF-5. The mechanism of increase of charge separations proposed in schematic representation as shown in Figure 5.

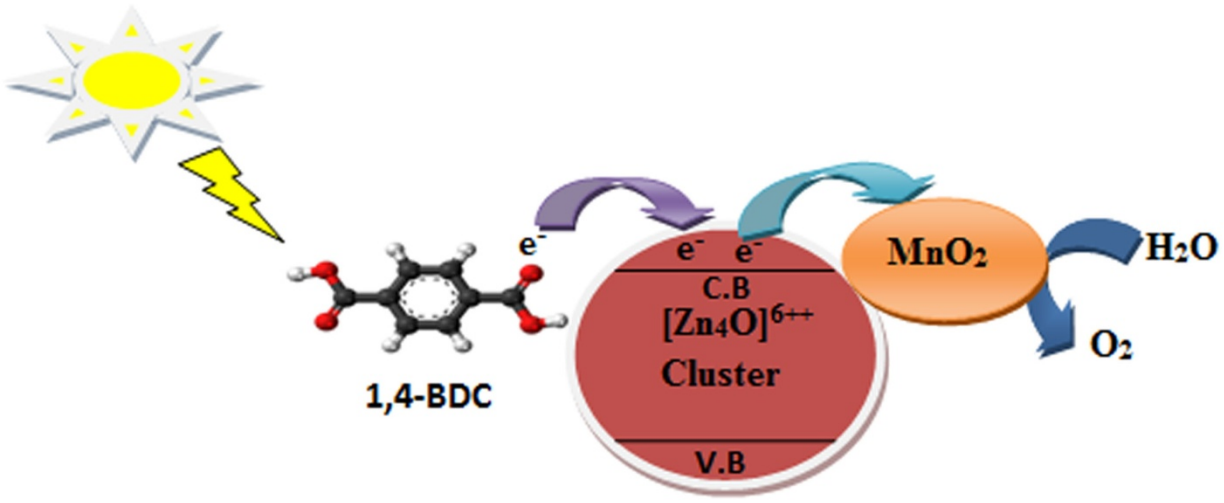

Figure 5: Schematic representation of increased charge separation and water splitting by MnO_2@MOF-5

Photoelectrochemical OER analysis

Firstly, photoelectrochemical studies towards OER are determined by cyclic voltammetry. CV curves of these electrodes are recorded using 1.0 M NaOH electrolyte both in presence of dark and under visible light at different scan rates (10, 20, 30, 40, 50 and 100mVs^{-1}) for MOF-5/NF and (5, 10, 20, 30, 40, 50, 60, 70, 80, 90 and 100mVs^{-1}) for MnO_2/NF and MnO_2@MOF-5/NF. It is found that all the working electrodes delivered almost zero current density in dark due to absence of OER activity. Figure 6(a) shows that MOF-5/NF generates no significant current density at various scan rates within RHE potential range of 0.2 to 1.2 V. Figures 6(b) and (c) showed CV curves for MnO_2/NF and MnO_2@MOF-5/NF electrodes under RHE potential range 1.0 to 1.6 V, in dark as well as in visible light. It is investigated from the CV curves of MnO_2/NF and MnO_2@MOF-5/NF that in the presence of visible light prominent increase in current density is observed, due to OER activity. However, pre-OER oxidation-reduction peaks are appeared in CV curves of MnO_2/NF and MnO_2@MOF-5/NF due to redox reaction of Ni(II)/Ni(III) [39]. In MnO_2/NF the oxidation and reduction peaks were appeared in range between 1.44 to 1.50 V and1.38 to 1.34 V, respectively. The CV curves of MnO_2@MOF-5/NF electrode showed that there are two oxidation peaks at various scan rates (10 to 100mVs^{-1}), first between 1.35 to 1.41V and then between 1.40 to 1.47 V, and only one reduction peak is observed between 1.28 to 1.20 V. It is revealed from the comparison

of CV curves of MOF-5/NF, MnO_2/NF and MnO_2@MOF-5/NF that MnO_2@MOF-5/NF has higher current density as compared to pure MOF-5/NF and MnO_2/NF due to hetero-junction formation between MnO_2/NF and central metallic cluster of MOF-5. Thus, synergistic effect and hetero-junction formation played a significant role to enhance the OER activity of MnO_2@MOF-5/NF as compared to all other synthesized samples. Inset of Figure 6 (b and c) represented the anodic and cathodic peak current density with respect to scan rate of MnO_2/NF and MnO_2@MOF-5/NF, respectively.

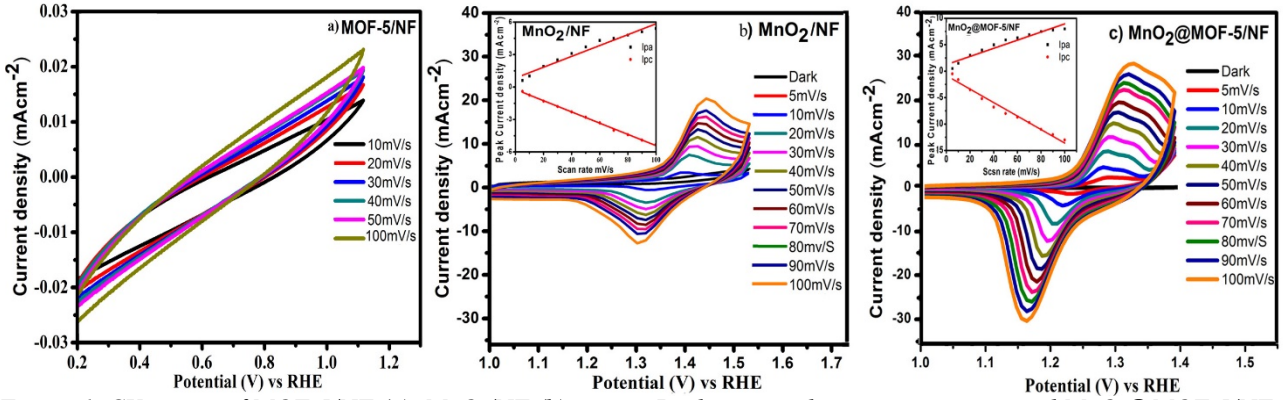

Figure 6: CV curves of MOF-5/NF (a), MnO_2/NF (b) inset is Peak current density vs scan rate and MnO_2@MOF-5/NF (c).Inset is Peak current density vs scan rateat different scan rates

The catalytic activity of MOF-5/NF, MnO_2/NF and MnO_2@MOF-5/NF electrodes are further evaluated by linear sweep voltammetry (LSV) in the presence of visible light in 1 M NaOH electrolyte, as shown in figure7a. As in CV, the anodic oxidative peak is observed in LSV of both MnO_2/NF and MnO_2@MOF-5/NF due to oxidation of $Ni^{2+} \rightarrow Ni^{3+}$ from Ni-foam. The LSV curve of MOF-5/NF electrode indicated that there is no significant generation of current density, even at very high overpotential it generated just 0.46 $mAcm^{-2}$ current density. For comparison between MnO_2/NF and MnO_2@MOF-5/NF, overpotential required to achieve 2 $mAcm^{-2}$current density is considered. It is observed that MnO_2@MOF-5/NF required low overpotential of 284 mV to achieve 2 $mAcm^{-2}$ current density. Whereas MnO_2/NF required 324 mV overpotential for 2 $mAcm^{-2}$. It is observed that MnO_2@MOF-5/NF delivered the benchmark of 10 $mAcm^{-2}$ at overpotential of 324 mV, which could be comparable and even less then some of reported Mn-based and other 3d transition metal based catalyst

for OER, represented by Table 1. Furthermore, to understand the kinetics of MnO_2@MOF-5/NF towards OER, Tafel plot is derived from LSV. The calculated Tafel slope values for MnO_2@MOF-5/NF is just 71 $mVdec^{-1}$, which is lowered then MnO_2/NF (157 $mVdec^{-1}$) and previously reported Mn-based materials such as MnO_2/Ni-Co carbonate precursor/NF (95 $mVdec^{-1}$) and $MnO_2/NiCo_2O_4$/NF (139 $mVdec^{-1}$) [40]. The lower Tafel slope value for MnO_2@MOF-5/NF indicated that it has more favorable electron transferred and improved catalytic activity as compared to MnO_2/NF and its rate-determining step for OER was the first electron transferred as shown below,

$$M + OH^- \rightarrow MOH + e^- \qquad (5)$$

Where, M is the catalytic active site [37-38].

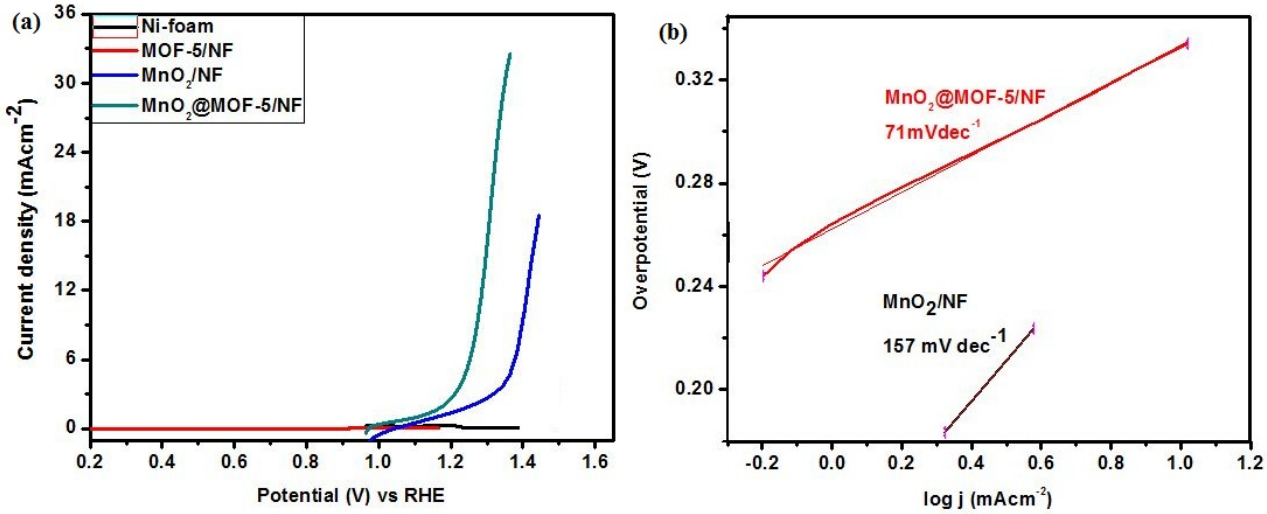

Figure 7: (a) LSV curves of MOF-5/NF, MnO_2/NF and MnO_2@MOF-5/NF; (b) Tafel plot for MnO_2/NF and MnO_2@MOF-5/NF

Table 1: The comparison of OER activity of MnO_2@MOF-5/NF with previously reported Mn-based and other 3d transition metal based OER catalyst.

Catalyst	Overpotential (mV) for $10mAcm^{-2}$ current density	Reference
Co^{2+}/MnO_2	360	ACS Catal. 2016, 6,7739.
Ni^{2+}/MnO_2	400	Angew Chem. Int. Ed. 2016, 55,10381
α- MnO_2	490	J. Am.Chm. Soc. 2014, 136, 11452.
Metal-ion doped MnO_2	390	Adv. Funct. Mater. 2017, 27, 1704083
CoMnP	330	J. Am.Chm. Soc. 2016, 138, 4006.
AuNi heterodimers	350	Small 2018, 14, 1703749
Co_9S_8@NOSC-900	330	Adv. Funct. Mater. 2016, 26, 4712.

Fe-doped mesoporous Co_3O_4	380	Chem. Commun. 2014, 50,10122.
α-MnO_2/$CDs_{0.25}$	352	Electrochim. Acta 2020, 337, 135823
MnO_2@MOF-5/NF	**324**	**This work.**

From the comparison of LSV curves it can be found that as a result of incorporation of MnO_2 into MOF-5 and due to synergistic effect, MnO_2@MOF-5/NF has improved OER catalytic activity over both pure MOF-5/NF and MnO_2/NF.

Stability of the synthesized materials during OER activity is evaluated by Chronoamperometric studies (Figure 8). It is observed that MnO_2@MOF-5/NF generated constant current density at constant applied voltage of 1.0 V for 6000 seconds in presence of visible light. Stability of MnO_2/NF was also constant during this time but it produced less current density.

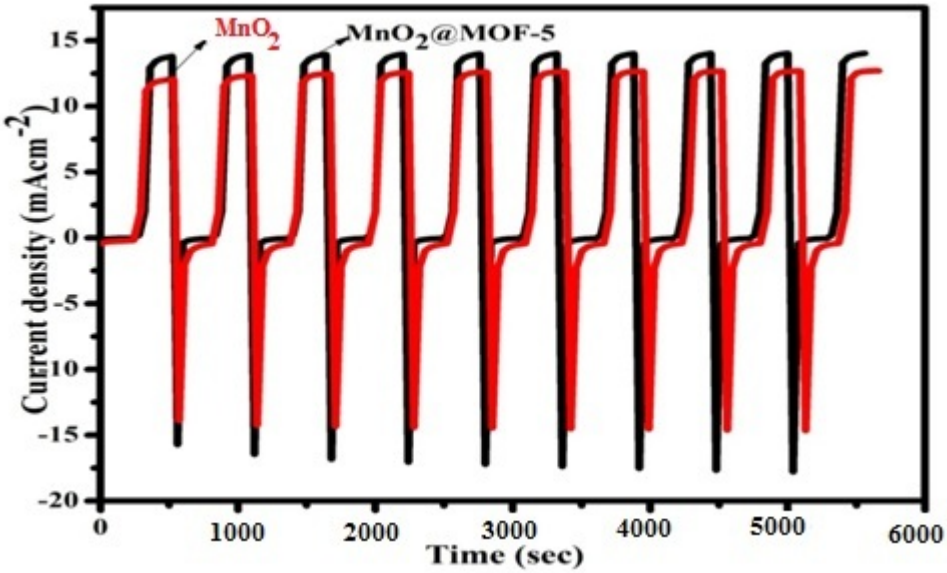

Figure 8: Chronoamperometric measurements of MnO_2/NF and MnO_2@MOF-5/NF at 1.0 V applied potential

Furthermore, the stability of MnO_2/NF andMnO_2@MOF-5/NF is studied by continuous CV sweeps in 1.0 M NaOH at a scan rate of 100 mV/s for 100 cycles. The CV curves revealed negligible degradation after 100 cycles of CV scanning, which confirmed the stability and durability of these electrodes. Figure S4 (a and b) represented the 1st and 100th cycle of CV curves at 100 mV/s of these electrodes and it revealed almost same curves with negligible difference.

Conclusions

MnO_2@MOF-5 composite has synthesized successfully by in-situ incorporation of pre-synthesized MnO_2 nanoparticles into MOF-5 and used as efficient OER catalyst. The MnO_2@MOF-5 composite has shown better OER activity as compared to MnO_2 and MOF-5. MnO_2@MOF-5 can

exposes active sites more effectively due to incorporation of MnO_2 nanoparticles and synergistic effect. The incorporation of MnO_2 nanoparticles leads a strong electron interaction between 1, 4-BDC (1,4-Benzenedicarbxylate), $[Zn_4O]^{6+}$ clusters and MnO_2 and further optimizes the charge transfer, so charge separation increased and electron-hole pair recombination decreased. Furthermore, binder's free formation of MnO_2@MOF-5/NF enhanced the electrical conductivity. The CV, LSV and Chronoamperometric results show that MnO_2@MOF-5 is an efficient OER catalyst and has more stability. This study will encourage for designing more versatile efficient materials by nanoparticles incorporation into MOFs for water splitting, fuel cells, supercapacitors and batteries.

Acknowledgements

Authors acknowledge Higher Education Commission (HEC) of Pakistan for financial support, Prof. Duncan H. Gregory from School of Chemistry, University of Glasgow, UK for providing lab facilities for this work under IRSIP and Dr. Muhammad Mazhar, Distinguished National Professor, Fatima Jinnah Women University, Rawalpindi and National University of Science, Islamabad for his valuable suggestions.

Conflict of interest:

Authors declare no conflict of interest.

References

1.Alfaifi B, Ullah H, Alfaifi S, Tahir A, Mallick T. Photoelectrochemical solar water splitting: From basic principles to sadvanced devices.Veruscript Functional Nanomaterials 2018; 2.

2. Stolarczyk J K, Bhattacharyya S, Polavarapu L, Feldmann J. Challenges and prospects in solar water splitting and CO_2 reduction with inorganic and hybrid nanostructures. ACS Catal 2018; 8:3602-3635.

3. Li R. Latest progress in hydrogen production from solar water splitting via photocatalysis, photoelectrochemical and photovoltaic-photoelectrochemical solutions. Chinese Journal of Catalysis 2017; 38: 5-12.

4. Yilmaz F, Balta T M, Selbas R. A review of solar based hydrogen production methods. Renewable and Sustainable Energy Review 2016;56:171-178.

5.Fujishima A, Honda K. Electrochemical photolysis of water at a semiconductor electrode. Nature 1972; 238: 37-38.

6.Maeda K, Damen K. Photocatalytic water splitting: recent progress and future challenges. J PhysChem Lett 2010; 1: 2655-61.

7. Suen N T, Hung S F, Quan Q, Zhang N, Xu Y J, Chen H M. Electrocatalysts for the oxygen evolution reaction: recent development and future perspectives. Chemical Society Review 2017, 46, 337-365.

8. Strasser P. Free electrons to molecular bonds and back: closing the energetic oxygen reduction (ORR) oxygen evolution reaction (OER) cycle using core-shell nanoelectrocatalysts. Accounts of Chemical Research 2016, 49, 2658.

9. Longhzhu L, Changhai L, Yangyang Q, Naotoshi M, Zhidong C. Convex-nanorods of a-Fe_2O_3/CQDs hetero-juctionphotoanode synthesized by a facile hydrothermal method for highly efficient water oxidation. Int J Hydrogen energy 2017; 42:19654-63

10. Junqi L, Jian Z, Hongjuan H, Weijia L. Controlled synthesis of Fe_2O_3 modified Ag-$_{010}BiVO_4$heterostructures with enhanced photoelectrochemical activity toward the dye degradation. Appl Surf Sci 2017; 399: 1-9.

11.Guanying D, Bin D, Lei L, Weiwei Z, Yujie L, Honglong S. Synthesis and their enhanced photoelectrochemical performance of ZnO nanoparticles-loaded CuO dandelion heterostructures under solar light. Appl Surf Sci 2017; 399: 86-94.

12. Kapelewski M T, Runcevski T, Tarver J D, Jiang H ZH, Hurst K E,Parilla P A, Ayala A, Gennett T, FitzGeraled SA, Brown CM, Long JR. Record high hydrogen storage capacity in the Metal Organic Framework Ni_2(m-dobdc) at Near-Ambient Temperatures. Chemistry of Materials 2018; 30:8179-8189.

13. Mansour O, Kawas G, Rasheed M A, Sakur A A. Applications of Metal Organic Framework (MOFs) to separation analytical techniques. Research J. Pharm and Tech 2018; 11:3514-3522.

14. Wee L H, Bonino F, Lamberti C, Bordiga S, Martens J A. Cr-MIL-101encapsulated Kegginphosphor tungstic acid as active nanomaterial for catalyzing the alcoholysis of styrene oxide. Green Chem 2014; 16: 1351-1357.

15.Corma A, Garcia H, iXamena F X L. Engineering metal organic framework for heterogeneous catalysis. Chem Rev 2010; 110: 4606- 4655.

16. Kreno LE, Leong K, Farha OK, Allendorf M, Van DuyneRP, Hupp JT. Metal organic framework materials as chemical sensors. Chem Rev 2012; 112: 1105-25.

17. Gomes SC, Luz I, iXamena FXL, Corma A, Garcia H. water stable Zr-benzenedicarboxylate metal organic framework as photocatalyst for hydrogen generation. Chemistry 2010; 16: 11133-8.

18.Peng R, Wu CM, Baltrusaitis J, Dimitrijevic NM, Rajh T, Koodali RT. Ultra-stable CdS incorporated Ti-MCM-48 mesoprous materials for efficient photocatalytic decomposition of water under visible light illumination. ChemCommun 2013; 49: 3221-3223.

19.Sugikawa K, Nagata S, Furukawa Y, Kokado K, Sada K. Stable and functional gold nanorod composites with a metal organic framework crystalline shell. Chem Mater 2013; 25:2565-2570.

20. He L, Liu Y, Liu J, Xiong Y, Zheng J, Liu Y, TangZ.Core shell noble metal@metal organic framework nanoparticles with highly selective sensing property. AngewChemInt Ed 2013; 52: 3741-3745.

21.Buso D, Jasieniak J, Lay M D H, Schiavuta P, Scopece P, Laird J, Amenitsch H, Hill A J,Falcaro P. Highly luminescent metal organic framework through quantum dot doping. Small 2012;8: 80-88.

22. Petit C, Bandosz T J. MOF-Graphite Oxide Composites:Combining the Uniqueness of Graphene Layers and Metal-Organic Frameworks. Adv Mater 2009; 21: 4753-4757.

23. Buso D, Nairn K M, Gimona M, Hill A J, Falcaro P. Fast synthesis of MOF-5 microcrystals using sol-gel SiO_2 nanoparticles. Chem Mater 2011; 23:929-934.

24. Meyer K, Ranocchiari M, Bokhoven J AV. Metal Organic framework for photocatalytic water splitting. Energy Environ Sci2015;8:1923-1937

25. Tian L, Zhai X, Wang X, Li Z. Advances in manganese-based oxides for oxygen evolution reaction. Journal of Materials Chemistry A 2020, 8, 14400-14414.

26. Tian L, Zhai X, Wang X, Pang X, Li J, Li Z. Morphology and phase transformation of α-MnO_2/MnOOH modulated by N-CDs for efficient electrocatalytic oxygen evolution reaction in alkaline medium. Electrochemica Acta 2020, 337, 135823-135832.

27. Li Z, Cai L, Song M, Shen Y, Wang X, Li J, Wang J, Wang P, Tian L. Ternary FeCoNi alloy nanoparticles in N-doped carbon nanotubes for efficient oxygen evolution reaction electrocatalysts. Electrochemica Acta 2020, 339, 13886-135894.

28.Kim K, Daniel G, Kessler V G, Seisenbaeve G A, Pol V G. Basic Medium Heterogeneous Solution Synthesis of α-MnO_2Nanoflakes as an Anode or Cathode in Half Cell Configuration (vs. Lithium) of Li-Ion batteries. Nanomaterials 2018;8: 608-619.

29. Lee H J, Park S, Kim H. Analysis of the effect of MnO_2 precipitation on the performance of Vanadium/Manganese Redox Flow Battery. J ElectrochemSoc 2018; 165: 952-956.

30. Chan Z M, Kitchaev D A, Weker J N, Schnedermann C, Lim K,Ceder G, Tumas W, Toney M F, Nacera D G. Electrochemical trapping of metastable Mn^{3+} ions for activation of MnO_2 oxygen evolution catalysts. PNAS 2018; 115: E5261-E5268

31. Eddaoudi M, Kim J, Rosi N, Vodak D, Wachter J, O'Keeffe M, Yaghi O M. Systematic design of pore size and functionality in isoreticular MOFs and their application in methane storage. Science 2002; 295: 469–472.

32. Chen Y, Duan Z, Min Y, Shao M, Zhao Y. Synthesis characterization and catalytic property of manganese dioxide with different structures. J Mater Sci Mater Electron 2011;22: 1162–1166

33.Rehman A, Tirmizi SA, Badshah A, Ammad H M, Jawad M, Abbas S M, Rana U A, Khan S D. Synthesis of highly stable MOF-5@MWCNTs nanocomposite with improved hydrophobic properties. Arabian Journal of Chemistry 2018; 11: 26-33.

34.Hafizovic J, Bjørgen M, Olsbye U, Dietzel PDC, Bordiga S, Prestipino C, Lamberti C, Lillerud KP. The inconsistency in adsorption properties and powder XRD data of MOF-5 rationalized by framework interpenetration and the presence of organic and inorganic species in the nanocavities. J Am ChemSoc2007; 129: 3612–3620.

35. Bordiga S, Lamberti C, Ricchiardi G, Regli L, Bonino F, Damin A, Lillerud KP, BjorgenM,Zecchina A. Electronic and vibrational properties of a MOF-5 metal-organic framework: ZnO quantum dot behavior. ChemCommun 2004;20: 2300–2301.

36. Hu Y H, Zhang L. Amorphization of metal organic framework MOF-5 at unusually low applied pressure. Phys Rev B 2010; 81: 174103 -174107.

37.Sabouni R, Kazemian H, Rohani S. A novel combined manufacturing technique for rapid production of IRMOF-1 using ultrasound and microwave energies. ChemEng J2010;165:966-973.

38. Yang L M, Fang G Y, Ma J, Granz E, Han S S. Band Gap Engineering of Paradigm MOF-5. Cryst. Gowth Des. 2014; 14: 2532-2541.

39. Xing J, Guo K, Zou Z, Cai M, Du J, Xu C.In situ growth of well-ordered NiFe-MOF-74 on Ni foam by Fe^{2+} induction as an efficient and stable electrocatalyst for water oxidation.Chem. Commun. 2018; 54: 7046-7049.

40. Yan K L, SHANG X, Gao W K, Dong B, Li X, Chi J Q, Liu Y R, Chai Y M, Liu C G. Ternary MnO_2/$NiCo_2O_4$/NF with hierarchical structure and synergistic interaction as efficient electrocatalysts for oxygen evolution reaction. J Alloys and Compounds 2017; 719: 314-321.